Pure-State Photon-Pair Source with a Long Coherence Time for Large-Scale Quantum Information Processing

Bo Li[1,2,3] Yu-Huai Li,[1,2,3,*] Yuan Cao[1,2,3] Juan Yin,[1,2,3] and Cheng-Zhi Peng[1,2,3]

[1]*Hefei National Laboratory for Physical Sciences at the Microscale and Department of Modern Physics, University of Science and Technology of China, Hefei, 230026 Anhui, China*

[2]*Shanghai Branch, CAS Center for Excellence in Quantum Information and Quantum Physics, University of Science and Technology of China, 201315 Shanghai, China*

[3]*Shanghai Research Center for Quantum Sciences, 201315 Shanghai, China*

The Hong-Ou-Mandel interference between independent photons plays a pivotal role in large-scale quantum networks involving distant nodes. Photons need to work in a pure state for indistinguishability to reach high-quality interference. Also, they need to have a sufficiently long coherence time to reduce the time-synchronization requirements in practical applications. In this paper, we discuss a scheme for generating a pure-state photon-pair source with a long coherence time in periodically poled potassium titanyl phosphate crystals. By selecting the appropriate pump laser and filter, we can simultaneously eliminate the frequency correlation of the parametric photons while achieving a long coherence time. We experimentally develop this pure-state photon-pair source of 780 nm on potassium titanyl phosphate crystals pumped by a 390-nm pulsed laser. The source provides a coherence time of tens of picoseconds, and it is shown to have the potential to be applied in long-distance quantum interference. Furthermore, we experimentally demonstrate the Hong-Ou-Mandel interference between two photon sources with visibility exceeding the classical limit.

I. INTRODUCTION

Photon-pair sources are essential in the field of quantum information processing, which includes quantum communication [1,2] quantum computation [3], and Bell tests [4,5]. Complex quantum communication protocols such as teleportation [6] and swapping [7] involve more than two photons, where interference is required between independent photon sources. Thus, independent photon-pair sources should be prepared with high spectral purity. To implement these schemes on a large scale, it is crucial for the coherence time of the photon source to be sufficiently long (on the order of picoseconds), which will help mitigate the challenges associated with time synchronization over long distances. Simultaneously, it is essential to thoroughly address other key parameters, such as brightness and purity. Moreover, source implementation should consider the flexibility and robustness required for practical applications.

Nowadays, the most extensively used approach to generate photon pairs is spontaneous parametric downconversion (SPDC) in nonlinear crystals [8]. The pulse duration, the material, thickness, and cut angle of a nonlinear medium, or the length and period of a periodically poled nonlinear medium should be carefully considered to deal with the group-velocity-match (GVM) issue [9]. In conventional multiphoton setups, β-barium borate or bismuth borate crystals with a thickness of a few millimeters are commonly used, resulting in a photon bandwidth of 3 nm (or 8 nm) [10–12]. This configuration, operated with a high-power (approximately-watt-level) and femtosecond (approximately-100-fs) pump laser, lacks flexibility when applied in practical field experiments or a power-starved scenario such as in satellites. With an approximately-100-fs pump pulse [10], the synchronization precision should be at the level of 10 fs between remote parties, which reaches the state-of-the-art technology that involves optical clocks [13], cavity-stabilized lasers [14], and frequency-comb-assisted time transfer [15], which are not currently practical. For practical applications, it is advisable to ensure a long coherence time of the source comparable to the practical time synchronization achieved through commercial atomic clocks or oven-protected crystal oscillators [16]. Typically, time-synchronization systems using these methods yield a precision of tens of picoseconds.

By taking advantage of the quasi-phase-matching (QPM), one can use periodically poled nonlinear crystals

————————
*liyuhuai@ustc.edu.cn

to provide a flexible approach for almost-arbitrary phase-matching angles and wavelengths [17]. Thus, with a collinear configuration, the crystal can be fairly thick for a high generation rate of photon pairs without unwanted walk-off. QPM-SPDC sources have a variety of applications, such as space-borne payloads [18–21] and air-borne payloads [22,23] in long-distance quantum communication and photonic boson sampling [24] in quantum computation. Many great efforts have been made concerning the telecom photon pairs generated from potassium titanyl phosphate (PPKTP) [25,26] for multiphoton applications. When one is preparing degenerate parametric photons at around 1560 nm in type-II PPKTP crystals, the GVM condition can intrinsically be satisfied. Thus, the time and frequency correlations between the signal and idler photons are naturally eliminated even without any filters. However, because of the wavelength increase, the emission rate of photon pairs in the telecom band is decreased compared with that of visible parametric photons [27]. PPKTP-based photon-pair sources with a wavelength of 780 nm, which are suitable for nonclassical interference, have been reported [28]. However, the configuration use a short crystal (1 mm) and ultrafast pump pulses (150 fs), leading to a short coherence time of approximately 1 ps.

In this paper, by carefully examining the GVM condition, we find that filtered SPDC sources can still be beneficial for application in field experiments with an acceptable loss. We show that a 780-nm photon-pair source with a bandwidth of 30 pm can be constructed by our carefully selecting the pump laser, nonlinear crystal parameters, and proper filters applied on the parametric photons. This implies that a coherence time of tens of picoseconds and a pair generation rate on the order of approximately 2×10^5 pairs per milliwatt per second can be reached. With such a configuration, a 30-mW pump laser with a repetition rate of 76 MHz is sufficient to produce approximately 0.1 photon pairs per pulse, which lower the requirement of a high-power pump condition. Furthermore, a proof-of-principle experiment involving Hong-Ou-Mandel (HOM) interference [29] between two heralded single-photon sources is performed to demonstrate the feasibility of the proposed method in multiphoton applications.

II. DESIGN OF THE PHOTON SOURCE

When one is developing a photon-pair source, it is crucial to consider the photon spectral emission and phase-matching conditions. The photon yield depends on several factors, including the wavelength used, the crystal's length, and the focusing parameters in bulk crystals. The phase-matching conditions affect the spectral distribution of the generated photons. Understanding these conditions is essential for establishing the ideal filtering approach and other specific applications.

A. General concepts

1. Spectral emission

According to the theory of the SPDC process in bulk crystals, in the case of a collinear emission with degenerate wavelength, the spectral generation rate of parametric photons can be written as follows [30]:

$$\frac{dP_s}{P_p d\omega_s} = \frac{\hbar d^2 L \omega_s^4}{2\pi c^4 \varepsilon_0 n_p^2} f(\lambda_s) = \frac{\hbar d^2}{2\pi c^4 \varepsilon_0} f(\lambda_s) \times \frac{1}{n_p^2} \times L\omega_s^4, \tag{1}$$

where ω_s is the angular frequency of signal photon, respectively, P_s is the signal-photon power integrated over all emission angles, d is the effective nonlinear coefficient, L is the crystal length, c is the speed of light in a vacuum, ε_0 is the permittivity of a vacuum, n_p is the refractive index of the pump laser in the crystal, P_p is the pump power, and $f(\lambda_s)$ is a geometry-related function, and it be regarded as a constant in this paper. The first term, $\hbar d^2 f(\lambda_s)/2\pi c^4 \varepsilon_0$, is a constant. The value of the second term, $1/n_p^2$, depends on ω_p. For a polarized photon transmission along the y axis in a PPKTP crystal, the refractive index varies from 1.844 to 1.727 for a wavelength range of 0.4-2.0 μm [31]. This variation is negligible, as it is less than 7%. As indicated in the last term, the spectral brightness is directly proportional to the crystal length and the fourth power of ω_s. Therefore, increasing the spectral brightness may be achieved by use of a longer crystal and a shorter wavelength. In our scheme, it should be noted that a filter will not impact the spectral emission. Thus, maximizing the initial spectral emission rate is imperative to increase the available photons with a narrow filter.

2. Spectral correlation

In this section we detail the spectral-correlation effect of the general SPDC process. Theoretically, the wave function of the parametric photons can be expressed as follows [32]:

$$|\psi\rangle = N \int\int d\omega_s d\omega_i f(\omega_s, \omega_i) \hat{a}_s^\dagger(\omega_s)\hat{a}_i^\dagger(\omega_i)|0\rangle, \tag{2}$$

where $\hat{a}_s^\dagger(\omega_s)$ and $\hat{a}_i^\dagger(\omega_i)$ are the photon creation operators for the signal and idler beams, respectively, $|0\rangle$ is a vacuum state, and N is a normalization constant. $f(\omega_s, \omega_i)$ is the joint spectral amplitude (JSA), which represents the spectral correlation between the signal and idler photons, and it can be expressed as the product of the pump-envelope function $\alpha(\omega_s, \omega_i)$ and the QPM function $\phi(\omega_s, \omega_i)$:

$$f(\omega_s, \omega_i) = \alpha(\omega_s + \omega_i)\phi(\omega_s, \omega_i). \tag{3}$$

In the case of pumping by a Gaussian-line-shaped laser with a central frequency of $\overline{\omega}_p$ and a bandwidth of σ_p, the

pump-envelope function can be written as follows:

$$\alpha(\omega_s + \omega_i) \propto \exp\left[-\frac{(\omega_s + \omega_i - \overline{\omega}_p)^2}{2\sigma_p^2}\right]. \qquad (4)$$

The phase-matching function is given as follows:

$$\phi(\omega_s, \omega_i) = \text{sinc}\left[\frac{L}{2}\Delta k\right], \qquad (5)$$

where $\Delta k = k_p - k_s - k_i - m2\pi/\Lambda$, L is the crystal length, k is the wave number, Λ is the poling period, and m is the order of QPM.

The spectral correlation of photon pairs is determined by the joint spectral intensity (JSI) $S(\omega_s, \omega_i) = |f(\omega_s, \omega_i)|^2$, which is the product of the pump-envelope intensity $|\alpha(\omega_s + \omega_i)|^2$ and the phase-matching intensity $|\phi(\omega_s, \omega_i)|^2$. When there is a strong correlation between the photons, the initial purity of the generated photon pair will be low. One way to quantify the purity of the photon pair is by use of Schmidt decomposition on the JSI (see Appendix A).

3. Filtering method

Various technical approaches are available to select the frequency mode, and thus increase the purity, one of which is use of cavity-enhanced-SPDC technology [33–41]. In this technique, the photon has a typical bandwidth of several hundred megahertz, making it well suited for quantum storage. There are studies focused on developing it toward long-range quantum communication [36,39]. However, manipulating cavity-enhanced SPDC is relatively complex, as it requires handling issues such as cavity design, stability, compensation, loss control, and mode selection. The current research limit is the source brightness and efficiency, making it less effective for practical long-range quantum communication.

In comparison, use of a narrow-bandwidth filter to tailor the broadband SPDC photons is a straightforward and flexible way to increase photon purity and coherence length. Supposing that the interference filter is a Gaussian-type filter with a bandwidth of σ, then its amplitude function is given in the following form:

$$g(\Delta\omega) = e^{-\Delta\omega^2/2\sigma^2}. \qquad (6)$$

By introducing this to both signal and idler photons, one can represent the filtered JSA as follows:

$$f'(\omega_s, \omega_i) = g(\omega_s - \overline{\omega}_s)g(\omega_i - \overline{\omega}_i)f(\omega_s, \omega_i). \qquad (7)$$

Similarly, the purity can be obtained by Schmidt decomposition, for an optimal filtering strategy.

B. Detailed design

Below we use a long PPKTP crystal as an example to analyze how to design the source.

In engineering a photon-pair source for practical multiphoton use, achieving high purity is crucial. This can be accomplished either by manipulating the natural SPDC condition to meet specific requirements or by filtering the spectrum afterwards. A proper filter not only increases the purity but also increases the coherence time. However, the use of filters may result in photon loss, which can be mitigated by selection of high-performance periodically poled crystals that possess a high initial photon flux.

The factors that affect spectral brightness are represented in Eq. (1). To achieve a high photon flux, a type-II PPKTP crystal with a length of 30 mm and a poling period of 7.825 µm is used. The crystal is designed for degenerate emission with a pump laser of 390 nm, and it is crucial that the pump beam is focused onto the center of the crystal with an appropriate waist. A loose focus increases the coupling efficiency, while a strong focus can increase the pair emission rate. A trade-off between coupling efficiency and emission rate is necessary depending on specific applications [24,42]. For further detailed analysis, see Refs. [17,27].

The pump-laser bandwidth is another important factor to consider. The bandwidth has less effect on the absolute photon emission, but it greatly affects the distribution of the JSI, and thus the final filter selection. In our scheme, we aim to preserve as many photons as possible, so an optimal bandwidth of around 10-15 pm is chosen at the lowest Schmidt number, as shown in Fig. 1. A lower Schmidt number represents a lower mode number in the initial spectrum, thus reducing the filtering loss. From this, the optimized bandwidth of the pump laser can be obtained.
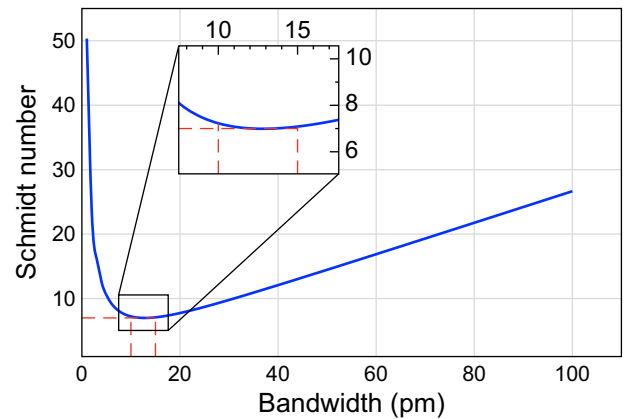

FIG. 1. Schmidt numbers with different pump bandwidths. A lower Schmidt number implies a greater natural purity of the generated photon pairs, and a smaller discarded fraction in filtering to reach a high purity. We show the interval with the lowest Schmidt number of approximately 7 (enlarged in the figure).
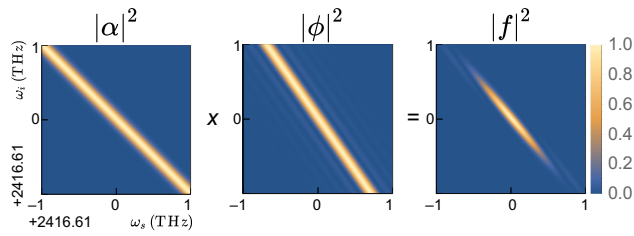
FIG. 2. Example of (a) the pump-envelope intensity, (b) the phase-matching intensity, and (c) the joint spectral intensity for a specific configuration: type-II PPKTP with a length of 30 mm, and a pump laser with a central wavelength of 390 nm and a pulse with an FWHM of 15 pm. A strong anticorrelation between the frequencies of the signal and idler photons can be seen in (c).

The corresponding JSI distribution is shown in Fig. 2. The slope of the pump-envelope intensity is fixed to 135° due to energy conservation, and its width is proportional to the bandwidth of the pump laser σ_p. The width of the phase-matching intensity is inversely proportional to the length of the PPKTP crystal L, while the slope is highly dependent on the wavelengths of the pump, signal, and idler photons. For the type-II SPDC process of 390 nm → 780 nm + 780 nm, the slope of the phase-matching intensity is 124.8°, which is close to the slope of the pump-envelope intensity, resulting in a highly correlated JSI. This type of photon source is intrinsically spectrally correlated. Thus, it cannot be directly applied in multiphoton engineering without first eliminating the correlation to achieve high purity.

To further decrease the Schmidt number to approach 1, a filtering method is proposed to be applied to the signal and idler photons symmetrically. As shown in Fig. 3, by application of a filter with an appropriate bandwidth (approximately 30 pm), the Schmidt number can be decreased to 1.05. The Schmidt-mode distributions for the filtered and the original frequency correlations are shown in Fig. 3(c).

According to the study by Meyer-Scott *et al.* [43], there is a trade-off between purity and heralding efficiency, which can be characterized by examining the JSI distribution. The filter heralding efficiency is defined as the ratio of the probability that both photons pass through their respective filters to the probability that each individual photon passes through its filter, denoted as $\eta_{f,s} = \Gamma_{\text{both}}/\Gamma_s$ and $\eta_{f,i} = \Gamma_{\text{both}}/\Gamma_i$ for the signal and idler photons, respectively. Figure 4 illustrates this trade-off for parametric photons. When the filter bandwidth is approximately 30 pm, the source achieves a high purity P of 0.95. However, the corresponding filter heralding efficiencies for the signal and idler photons reduce to 55.6% and 46.5%, respectively, with an average of 50.8%.

Table I presents optimal parameters of the filtered-SPDC process. The second column presents data measured with 30-mm bulk PPKTP crystals. The typical generation rate
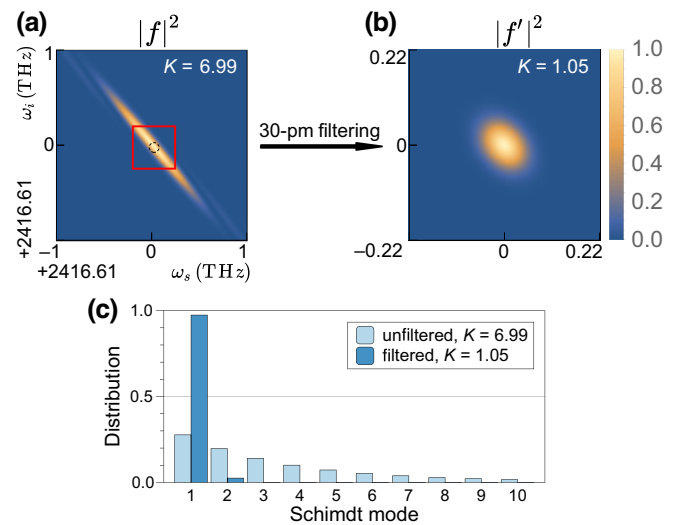

FIG. 3. Frequency correlation and Schmidt mode for the signal and idler photons. (a) The original JSI is highly correlated in frequency, with a Schmidt number of $K = 6.99$. (b) By filtering both the signal and idler photons with a 30-pm filter, the frequency correlation is almost completely removed, where the Schmidt number $K = 1.05$. (c) Comparison of the Schmidt-mode distributions for the original and the filtered JSI.

is 3.1×10^6 pairs per milliwatt per second and the bandwidths of idler and signal photons are 0.26 and 0.21 nm, respectively. The heralding efficiency is 20%, which includes the single-mode coupling efficiency of about 40% and a typical Si-detector efficiency of about 50%. The third column presents the predicted data with an ideal 30-pm filter applied symmetrically on both photons. The
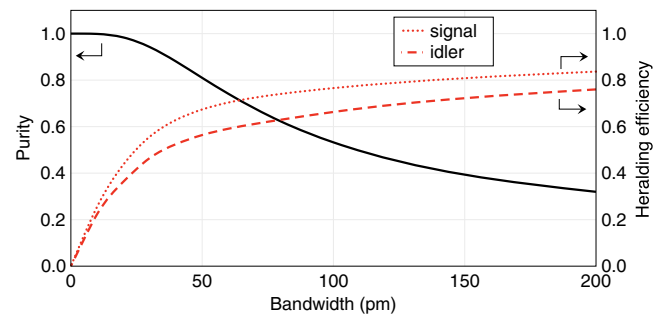

FIG. 4. Relationship between filter bandwidth and spectral purity, and the heralding efficiency for signal and idler photons. The filter is applied symmetrically to both signal and idler photons. As the filter becomes narrower, the purity (indicated by a solid black line) increases gradually from a low level to 1. However, simultaneously, the heralding efficiency (indicated by dashed and dotted red lines) decreases toward 0. Therefore, one must consider the trade-off between the purity and the heralding efficiency. For our application, an optimal filter bandwidth of roughly 30 pm is recommended, as this allows the purity to reach 0.95.

TABLE I. Optimal parameters for filtered SPDC.

Parameter	Without filter	With filter[a]
Pump power (mW)	30	30
$\Delta\lambda_p$ (nm)	0.015	0.015
$\Delta\lambda_s$ (nm)	0.21	0.03
$\Delta\lambda_i$ (nm)	0.26	0.03
Generation rate (s^{-1})	93.9×10^6	6.0×10^6
Coincidence rate (s^{-1})	3.75×10^6	0.2374×10^6
Heralding efficiency	20.0%	10.2%
$\bar{n}$[b]		0.079
Purity	0.14	0.95

[a]Ideal Gaussian filters are symmetrically applied on both signal and idler photons.
[b]Average photon number per pulse with the repetition rate set as 76 MHz.

filtered SPDC designed in this work requires a pump power of approximately 30 mW to produce an average photon number $\bar{n}$ of approximately 0.08. The twofold-coincidence rate has the potential to reach 237,000 counts per second. Our analysis indicates that filtered SPDC is still feasible in creating high-purity photon sources, which could have important implications for quantum information processing.

It is worth noting that waveguides are emerging as a practical alternative to bulk crystals in the field of photonics [44,45]. By use of long waveguides instead of bulk crystals, photon emission in SPDC can be increased by 1 order of magnitude or more. This increase is attributed to waveguides offering a greater confinement of the pump field, which leads to an increased photon-pair emission rate. Advancements in waveguide technology are anticipated to address concerns regarding the uniformity of long-crystal manufacturing, the efficiency of fiber coupling, and integration with free-space optics, which ultimately will pave the way for more-versatile applications.

In recent years, novel quantum photon sources, such as semiconductor quantum dots [46] and atomic ensembles [47–49], have emerged as a promising way to reach high brightness, high purity, and a long coherence time, which are essential for many quantum applications. The semiconductor-chip construction is complex and requires a low-temperature bath. While semiconductor quantum dots offer a near-perfect solution to the problem of low average photon number per excitation pulse, they are still in early development stages and have not yet surpassed mature SPDC technology in terms of flexibility and simplicity.

III. EXPERIMENTAL IMPLEMENTATION

On the basis of the above analysis, we experimentally realize a frequency-uncorrelated photon-pair source. We use a type-II PPKTP crystal of $1 \times 2 \times 30$ mm^3 for SPDC. The incident laser is focused with a waist diameter of

approximately 50 μm at the center of the PPKTP crystal. For the polarization, the pump and signal photons are adjusted to be along the crystal y axis, while the idler photons are adjusted to be along the z axis. Thus, the signal and idler photons can be separated by a polarized beam splitter, then coupled into single-mode fibers, and then detected by Si avalanche photodiodes.

To perform the experiment, a pump laser with a pulse width of approximately 15 ps is required. Unfortunately, we do not have access to such a laser. To address this requirement, we modify a femtosecond laser into a transform-limited picosecond laser using a filtering approach. As illustrated on the left in Fig. 5, the femtosecond pulsed laser with a wavelength of 780 nm is frequency-doubled by a 1-mm-thick lithium triborate crystal to generate a pulsed laser of 390 nm. The 780-nm femtosecond pulse comes from a Ti:sapphire laser with a repetition rate of 76 MHz. The 390-nm laser has a pulse with a full width at half maximum (FWHM) of 1.6 nm and an average power of 1.6 W. An air-spaced Fabry-Perot (FP) cavity with a finesse of 20 and an FWHM of 15 pm is selected as the narrow filter. The free spectral range of the FP filter is approximately 1.6 nm. Thus, coarse filtering is necessary to cover the range. Another consideration is the high-power femtosecond laser; we use a combination of a pair of dispersing prisms with dispersion coefficient $d\theta/d\lambda = 0.65$ mrad/nm and a slit as the coarse filter. Before it enters the first prism, the pump beam is expanded to a diameter of approximately 5 mm and a divergence angle of approximately 100 μrad by the lens. An adjustable slit is placed at the focal point to block any unwanted spectra. Afterwards, the beam is reshaped, collimated, and then passed through the FP cavity for fine filtering. According to the time-bandwidth-product limit, the final pump pulse corresponds to a pulse width of approximately 15 ps. The remaining available pump power is approximately 800 μW in total.

To increase the spectral purity of parametric photons, FP cavities with an FWHM of 30 pm and a finesse of 20 are used for filtering purposes. To assess the purity of the parametric photons, the second-order autocorrelation function $g^{(2)}(t)$ is measured in a Hanbury Brown–Twiss-like configuration [50], where photon coincidence is detected after a balanced beam splitter. The purity is related to the second-order autocorrelation function through the expression $g^{(2)}(0) = 1 + P$, where P denotes the purity. For an ideal decorrelated state, $g^{(2)}(0) = 2$ with $P = 1$, while a strongly correlated state exhibits Poissonian statistics with $g^{(2)}(0) = 1$ and $P = 0$. In this study, numerical estimates indicate that the spectral purity for perfectly filtering the signal photons $P_s = 0.7$ and for perfectly filtering the idler photons $P_i = 0.9$. The measured value of $g^{(2)}(0)$ is 1.01 ± 0.02 for unfiltered photons, indicating a very low purity. When the filter is applied to the idler photons, $g^{(2)}(0)$ increases to 1.72 ± 0.02, indicating P_i of approximately
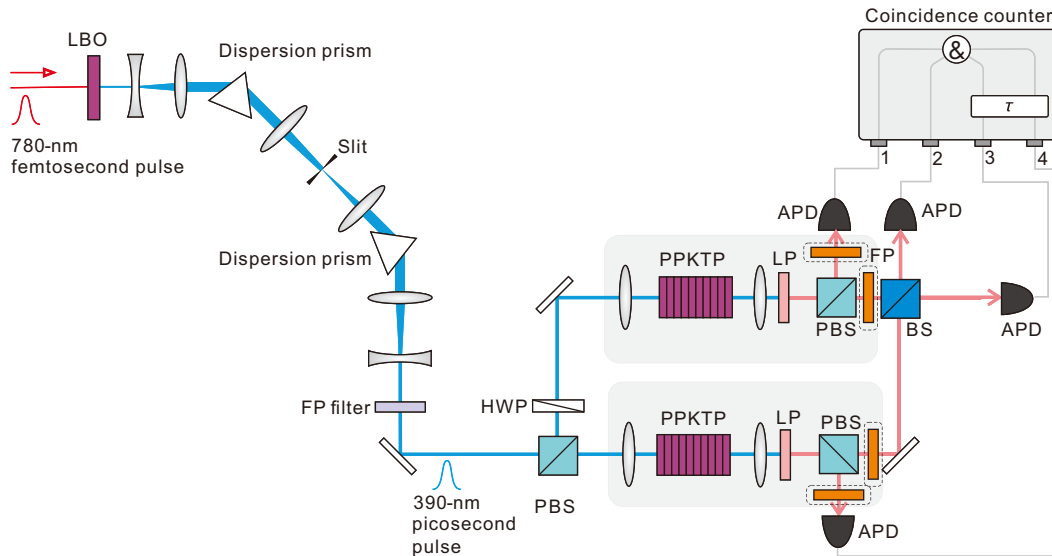
FIG. 5. Experimental demonstration of HOM interference. τ is the digital delay applied to photons 3 and 4. APD, Si avalanche photodiode with a detection efficiency of approximately 0.5; BS, 50:50 nonpolarizing beam splitter; HWP, half-wave plate; LBO, 1-mm-thick lithium triborate; LP, long-pass filter to block 390-nm photons; PBS, polarizing beam splitter.

0.72. To further increase the purity, another filter can be applied to the signal photons. It is estimated that the purity could reach as high as 0.95 in theory when both sets of photons are filtered.

After the filtering process, the observed coincidence count rate is 1.5×10^3 pairs per milliwatt per second, corresponding to an estimated photon-pair generating rate of 2×10^5 pairs per milliwatt per second (approximately 0.003 pairs per milliwatt per pulse). For most multiphoton experiments and applications, considering the signal-to-noise ratio, the optimized generating rate of the parametric photon pair is less than 0.1 per pulse; hence, a 30-mW pump laser is sufficient. The measured heralding efficiency of each parametric photon is approximately 4.3%, which is lower than the predicted value listed in Table I. The extra loss can be attributed to the spectral line shape of the FP cavity, the transmittance, and the distortion of the wave front by the cavity. By improvement of the filtering performance and increase of the pump power, a higher coincidence count rate can be expected in the future.

HOM interference is one direct way to verify the purity of an SPDC photon-pair source. The theory behind HOM interference can be found in Appendix B. It should be noted that spectral correlation is associated with the joint distribution of photon pairs. HOM interference is heralded by the idler photons, and filtering them can increase spectral purity, leading to an increase in the visibility of the signal photon's HOM interference. We build an HOM-interference configuration by preparing and combining two photon-pair sources, as shown on the right in Fig. 5. The idler photons work as triggers, and the signal photons are combined on a beam splitter for interference.

A thermoelectric cooler controls the temperature of each PPKTP crystal to ensure that the signal (idler) photons have the same central wavelength. All the arrival times of the photons are recorded by a time-digital converter to generate the fourfold-coincidence events. When the signal photons are indistinguishable in all degrees of freedom,
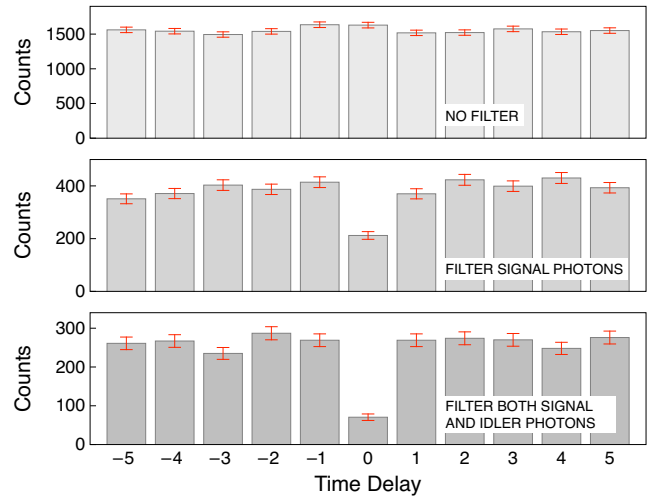

FIG. 6. Fourfold-coincidence counts with different time delays. The x axis represents the number of delayed pulse intervals. Since the repetition rate of the pump laser is 76 MHz, the interval of each pulse is 13.16 ns. Without the purification by filters, the visibility of HOM interference is almost zero. When both signal and idler photons are filtered by the FP filter with an FWHM of 30 pm, the visibility increases to 73.5%, exceeding the classical limit.

they bunch and leave the same port of the beam splitter. Thus, the fourfold-coincidence rate is ideally reduced to near zero.

Digital delay scanning is used to evaluate the visibility of HOM interference in the experiment. Before we calculate the fourfold-coincidence rate, a digital time delay τ is applied to two of the detectors, as shown in Fig. 5. The digital time delay is set as a sequence of integer multiples of the pulse interval. The fourfold-coincidence counts are displayed with the different digital time delays τ, and the corresponding experimental results are presented in Fig. 6. When unfiltered, HOM interference results in low visibility close to zero. We filter only the signal photons with the FP filter and leave the trigger photons unfiltered. Thus, the central bin is relatively decreased, and the visibility increases to $(46.01 \pm 2.95)\%$. Further, when the photons of the four paths are all filtered by the FP filters, the visibility reaches $(73.48 \pm 2.38)\%$, exceeding the classical limit of 0.5 [51,52], which provides solid evidence of the nonclassical interference between the two photon-pair sources.

IV. CONCLUSION

In summary, using a filtering method, we propose an approach for building a frequency-uncorrelated photon-pair source at 780 nm. Then, we experimentally realize this approach and show its potential in multiphoton applications by verifying HOM interference. The corresponding coherence time of the photon source is as long as tens of picoseconds, which is suitable for large-scale multiphoton applications in which clocks are required to be maintained and independently synchronized in remote parties. In the future, by increasing our configuration efficiency and updating the pump laser, we hope to develop the photon-pair source into a quantum communication application for long-distance channels.

Furthermore, the filtered-SPDC technique presented in this study can be applied to research in the telecom-frequency regime. The spectral brightness of SPDC decreases significantly as the wavelength increases. To overcome this limitation and achieve high brightness and a long coherence length, ultrabright SPDC sources based on periodically poled lithium niobate waveguides can be explored with use of the approach discussed in this paper. Furthermore, commercial telecom dense-wavelength-division-multiplexing technologies can be combined for increased versatility in constructing a multiplexed photon source, as demonstrated in previous studies [53,54].

ACKNOWLEDGMENTS

APPENDIX A: SCHMIDT DECOMPOSITION

The purity of the photons is defined as $P_s = \mathrm{Tr}(\hat{\rho}_s^2)$, where $\hat{\rho}_s = \mathrm{Tr}_i(|\Psi\rangle\langle\Psi|)$ is the reduced density operator of the signal [55]. The factorability of the JSA determines the purity. When the JSA results in a strong correlation, Schmidt decomposition of the JSA can be used to quantify the purity [56]. The JSA can be expressed as follows:

$$f(\omega_s, \omega_i) = \sum_k \sqrt{\lambda_n} u_k(\omega_s) v_k(\omega_i), \qquad (A1)$$

where $u_k(\omega_s)$ and $v_k(\omega_i)$ are two orthogonal basis sets of spectral functions, known as Schmidt modes, and λ_n is the weight of the Schmidt mode, where $\sum_n \lambda_n = 1$. The Schmidt number K is defined as follows:

$$K = \frac{1}{\sum_n \lambda_n^2}. \qquad (A2)$$

K is an indicator of entanglement. It represents the number of Schmidt modes existing in the two-photon states. The spectral purity is the inverse of the Schmidt number K:

$$P = P_s = P_i = \frac{1}{K}. \qquad (A3)$$

For a two-photon state $|\psi\rangle$ not correlated in the spectrum, the JSA can be written in a completely factorizable form:

$$f(\omega_s, \omega_i) = f_s(\omega_s) f_i(\omega_i). \qquad (A4)$$

Thus, $K = 1$.

For the spectral-correlation case, to calculate the numerical results for the Schimdt mode, we can discretize the spectrum. The JSA can be expressed in a large square matrix F. The matrix element F_{mn} of the mth row and the nth column is the discrete frequency value of $f(\omega_{s,m}, \omega_{i,n})$, where $\omega_{s,m}$ and $\omega_{i,n}$ are discrete frequencies. The Singular-value decomposition can decompose the matrix F into the following:

$$F = UDV = U \begin{bmatrix} d_1 & & \\ & d_2 & \\ & & \ddots \end{bmatrix} V, \qquad (A5)$$

where U and V are unitary matrices, where U depends on ω_s and V depends on ω_i. The diagonal matrix D needs to

be normalized with a coefficient $1/\sum d_n^2$. The matrix of the weight of the Schmidt mode is then

$$\begin{bmatrix} \lambda_1 & & \\ & \lambda_2 & \\ & & \ddots \end{bmatrix} = \frac{1}{\sum d_n^2} \begin{bmatrix} d_1^2 & & \\ & d_2^2 & \\ & & \ddots \end{bmatrix}. \quad \text{(A6)}$$

APPENDIX B: HOM-INTERFERENCE THEORY

HOM interference play an essential role in revealing the neoclassical multiphoton phenomenon. Its visibility is directly related to the purity of the photon source. Down-converted photon pairs can serve as a single-photon source, where one of the photons (idler in this work) serves as a trigger. HOM interference can be arranged by combining two independent heralded sources on a beam splitter. The fourfold-coincidence probability can be written as follows [57]:

$$P(t) = \int d\omega_{s_1} d\omega_{s_2} d\omega_{i_1} d\omega_{i_2} |f'(\omega_{s_1}, \omega_{i_1}) f'(\omega_{s_2}, \omega_{i_2})$$
$$- f'(\omega_{s_2}, \omega_{i_1}) f'(\omega_{s_1}, \omega_{i_2}) e^{-i(\omega_{s_2} - \omega_{s_1})t}|^2, \quad \text{(B1)}$$

where t denotes the path delay between two independent sources.

When the independent single photons are indistinguishable, HOM interference generates a dip in the fourfold coincidence when the time delay is 0. Also, the visibility is defined as follows:

$$V = \frac{P(\infty) - P(0)}{P(\infty)} = \mathcal{E}/\mathcal{A}, \quad \text{(B2)}$$

where

$$\mathcal{A} = \int d\omega_{s_1} d\omega_{s_2} d\omega_{i_1} d\omega_{i_2} \left| f'(\omega_{s_1}, \omega_{i1}) f'(\omega_{s2}, \omega_{i2}) \right|^2 \quad \text{(B3)}$$

and

$$\mathcal{E} = \int d\omega_{s_1} d\omega_{s_2} d\omega_{i_1} d\omega_{i_2} f'(\omega_{s1}, \omega_{i1}) f'(\omega_{s2}, \omega_{i2})$$
$$\times f'^*(\omega_{s1}, \omega_{i2}) f'^*(\omega_{s2}, \omega_{i1}), \quad \text{(B4)}$$

where f'^* signifies a conjugate function.

Visibility is theoretically equal to the state purity, $V = P = 1/K$ [58], which is the straightforward method for evaluating spectral purity.

---

[1] A. K. Ekert, Quantum Cryptography Based on Bell's Theorem, Phys. Rev. Lett. **67**, 661 (1991).

[2] C. H. Bennett, G. Brassard, and N. D. Mermin, Quantum Cryptography without Bell's Theorem, Phys. Rev. Lett. **68**, 557 (1992).

[3] E. Knill, R. Laflamme, and G. J. Milburn, A scheme for efficient quantum computation with linear optics, Nature **409**, 46 (2001).

[4] J. S. Bell, On the Einstein Podolsky Rosen paradox, Phys. Phys. Fiz. **1**, 195 (1964).

[5] J. F. Clauser, M. A. Horne, A. Shimony, and R. A. Holt, Proposed Experiment to Test Local Hidden-Variable Theories, Phys. Rev. Lett. **23**, 880 (1969).

[6] D. Bouwmeester, J.-W. Pan, K. Mattle, M. Eibl, H. Weinfurter, and A. Zeilinger, Experimental quantum teleportation, Nature **390**, 575 (1997).

[7] J. W. Pan, D. Bouwmeester, H. Weinfurter, and A. Zeilinger, Experimental Entanglement Swapping: Entangling Photons That Never Interacted, Phys. Rev. Lett. **80**, 3891 (1998).

[8] D. C. Burnham and D. L. Weinberg, Observation of Simultaneity in Parametric Production of Optical Photon Pairs, Phys. Rev. Lett. **25**, 84 (1970).

[9] W. P. Grice and I. A. Walmsley, Spectral information and distinguishability in type-II down-conversion with a broadband pump, Phys. Rev. A: At. Mol. Opt. Phys. **56**, 1627 (1997).

[10] X.-C. Yao, T.-X. Wang, P. Xu, H. Lu, G.-S. Pan, X.-H. Bao, C.-Z. Peng, C.-Y. Lu, Y.-A. Chen, and J.-W. Pan, Observation of eight-photon entanglement, Nat. Photon. **6**, 225 (2012).

[11] X.-L. Wang, L.-K. Chen, W. Li, H.-L. Huang, C. Liu, C. Chen, Y.-H. Luo, Z.-E. Su, D. Wu, Z.-D. Li, H. Lu, Y. Hu, X. Jiang, C.-Z. Peng, L. Li, N.-L. Liu, Y.-A. Chen, C.-Y. Lu, and J.-W. Pan, Experimental Ten-Photon Entanglement, Phys. Rev. Lett. **117**, 210502 (2016).

[12] H.-S. Zhong, Y. Li, W. Li, L.-C. Peng, Z.-E. Su, Y. Hu, Y.-M. He, X. Ding, W. Zhang, H. Li, L. Zhang, Z. Wang, L. You, X.-L. Wang, X. Jiang, L. Li, Y.-A. Chen, N.-L. Liu, C.-Y. Lu, and J.-W. Pan, 12-Photon Entanglement and Scalable Scattershot Boson Sampling with Optimal Entangled-Photon Pairs from Parametric Down-conversion, Phys. Rev. Lett. **121**, 250505 (2018).

[13] A. D. Ludlow, M. M. Boyd, J. Ye, E. Peik, and P. O. Schmidt, Optical atomic clocks, Rev. Mod. Phys. **87**, 637 (2015).

[14] T. Kessler, C. Hagemann, C. Grebing, T. Legero, U. Sterr, F. Riehle, M. J. Martin, L. Chen, and J. Ye, A sub-40-mHz-linewidth laser based on a silicon single-crystal optical cavity, Nat. Photon. **6**, 687 (2012).

[15] J.-D. Deschênes, L. C. Sinclair, F. R. Giorgetta, W. C. Swann, E. Baumann, H. Bergeron, M. Cermak, I. Coddington, and N. R. Newbury, Synchronization of Distant Optical Clocks at the Femtosecond Level, Phys. Rev. X **6**, 021016 (2016).

[16] Y. Cao, *et al.*, Long-Distance Free-Space Measurement-Device-Independent Quantum Key Distribution, Phys. Rev. Lett. **125**, 260503 (2020).

[17] A. Fedrizzi, T. Herbst, A. Poppe, T. Jennewein, and A. Zeilinger, A wavelength-tunable fiber-coupled source of narrowband entangled photons, Opt. Express **15**, 15377 (2007).

[18] J. Yin, *et al.*, Satellite-to-Ground Entanglement-Based Quantum Key Distribution, Phys. Rev. Lett. **119,** 200501 (2017).

[19] J. Yin, *et al.*, Entanglement-based secure quantum cryptography over 1,120 kilometres, Nature **582,** 501 (2020).

[20] J. Yin, *et al.*, Satellite-to-Ground Entanglement-Based Quantum Key Distribution, Phys. Rev. Lett. **119,** 200501 (2017).

[21] Z. Tang, R. Chandrasekara, Y. C. Tan, C. Cheng, K. Durak, and A. Ling, The photon pair source that survived a rocket explosion, Sci. Rep. **6,** 25603 (2016).

[22] H.-Y. Liu, X.-H. Tian, C. Gu, P. Fan, X. Ni, R. Yang, J.-N. Zhang, M. Hu, J. Guo, X. Cao, X. Hu, G. Zhao, Y.-Q. Lu, Y.-X. Gong, Z. Xie, and S.-N. Zhu, Drone-based entanglement distribution towards mobile quantum networks, Natl. Sci. Rev. **7,** 921 (2020).

[23] H.-Y. Liu, X.-H. Tian, C. Gu, P. Fan, X. Ni, R. Yang, J.-N. Zhang, M. Hu, J. Guo, X. Cao, X. Hu, G. Zhao, Y.-Q. Lu, Y.-X. Gong, Z. Xie, and S.-N. Zhu, Optical-Relayed Entanglement Distribution Using Drones as Mobile Nodes, Phys. Rev. Lett. **126,** 020503 (2021).

[24] H. S. Zhong, *et al.*, Quantum computational advantage using photons, Science 370, 1460 (2021). ArXiv:2012.01625,

[25] R.-B. Jin, R. Shimizu, K. Wakui, M. Fujiwara, T. Yamashita, S. Miki, H. Terai, Z. Wang, and M. Sasaki, Pulsed Sagnac polarization-entangled photon source with a PPKTP crystal at telecom wavelength., Opt. Express **22,** 11498 (2014).

[26] R.-B. Jin, M. Takeoka, U. Takagi, R. Shimizu, and M. Sasaki, Highly efficient entanglement swapping and teleportation at telecom wavelength, Sci. Rep. **5,** 9333 (2015).

[27] A. Ling, A. Lamas-Linares, and C. Kurtsiefer, Absolute emission rates of spontaneous parametric down-conversion into single transverse Gaussian modes, Phys. Rev. A **77,** 043834 (2008).

[28] T. Scheidl, F. Tiefenbacher, R. Prevedel, F. Steinlechner, R. Ursin, and A. Zeilinger, Crossed-crystal scheme for femtosecond-pulsed entangled photon generation in periodically poled potassium titanyl phosphate, Phys. Rev. A **89,** 042324 (2014).

[29] C. K. Hong, Z. Y. Ou, and L. Mandel, Measurement of Subpicosecond Time Intervals between Two Photons by Interference, Phys. Rev. Lett. **59,** 2044 (1987).

[30] M. Fiorentino, S. M. Spillane, R. G. Beausoleil, T. D. Roberts, P. Battle, and M. W. Munro, Spontaneous parametric down-conversion in periodically poled KTP waveguides and bulk crystals, Opt. Express **15,** 7479 (2007).

[31] K. Kato and E. Takaoka, Sellmeier and thermo-optic dispersion formulas for KTP, Appl. Opt. **41,** 5040 (2002).

[32] W. P. Grice, A. B. U'Ren, and I. A. Walmsley, Eliminating frequency and space-time correlations in multiphoton states, Phys. Rev. A **64,** 063815 (2001).

[33] X.-H. Bao, Y. Qian, J. Yang, H. Zhang, Z.-B. Chen, T. Yang, and J.-W. Pan, Generation of Narrow-Band Polarization-Entangled Photon Pairs for Atomic Quantum Memories, Phys. Rev. Lett. **101,** 190501 (2008).

[34] M. Scholz, L. Koch, R. Ullmann, and O. Benson, Single-mode operation of a high-brightness narrow-band single-photon source, Appl. Phys. Lett. **94,** 201105 (2009).

[35] E. Pomarico, B. Sanguinetti, C. I. Osorio, H. Herrmann, and R. T. Thew, Engineering integrated pure narrow-band photon sources, New J. Phys. **14,** 033008 (2012).

[36] F. Monteiro, A. Martin, B. Sanguinetti, H. Zbinden, and R. T. Thew, Narrowband photon pair source for quantum networks, Opt. Express **22,** 4371 (2014).

[37] K.-H. Luo, H. Herrmann, S. Krapick, B. Brecht, R. Ricken, V. Quiring, H. Suche, W. Sohler, and C. Silberhorn, Direct generation of genuine single-longitudinal-mode narrow-band photon pairs, New J. Phys. **17,** 073039 (2015).

[38] M. Rambach, A. Nikolova, T. J. Weinhold, and A. G. White, Sub-megahertz linewidth single photon source, APL Photon. **1,** 096101 (2016).

[39] K. Niizeki, K. Ikeda, M. Zheng, X. Xie, K. Okamura, N. Takei, N. Namekata, S. Inoue, H. Kosaka, and T. Horikiri, Ultrabright narrow-band telecom two-photon source for long-distance quantum communication, Appl. Phys. Express **11,** 042801 (2018).

[40] A. Moqanaki, F. Massa, and P. Walther, Novel single-mode narrow-band photon source of high brightness tuned to cesium D2 line, APL Photon. **4,** 090804 (2019).

[41] O. Slattery, L. Ma, K. Zong, and X. Tang, Background and review of cavity-enhanced spontaneous parametric down-conversion, J. Res. Natl. Inst. Stand. Technol. **124,** 124019 (2019).

[42] M.-H. Li, C. Wu, Y. Zhang, W.-Z. Liu, B. Bai, Y. Liu, W. Zhang, Q. Zhao, H. Li, Z. Wang, L. You, W. J. Munro, J. Yin, J. Zhang, C.-Z. Peng, X. Ma, Q. Zhang, J. Fan, and J.-W. Pan, Test of Local Realism into the Past without Detection and Locality Loopholes, Phys. Rev. Lett. **121,** 080404 (2018).

[43] E. Meyer-Scott, N. Montaut, J. Tiedau, L. Sansoni, H. Herrmann, T. J. Bartley, and C. Silberhorn, Limits on the heralding efficiencies and spectral purities of spectrally filtered single photons from photon-pair sources, Phys. Rev. A **95,** 061803(R) (2017).

[44] M. Halder, A. Beveratos, R. T. Thew, C. Jorel, H. Zbinden, and N. Gisin, High coherence photon pair source for quantum communication, New J. Phys. **10,** 023027 (2008).

[45] Z. H. Levine, J. Fan, J. Chen, A. Ling, and A. Migdall, Heralded, pure-state single-photon source based on a potassium titanyl phosphate waveguide, Opt. Express **18,** 3708 (2010).

[46] H. Wang, H. Hu, T.-H. Chung, J. Qin, X. Yang, J.-P. Li, R.-Z. Liu, H.-S. Zhong, Y.-M. He, X. Ding, Y.-H. Deng, Q. Dai, Y.-H. Huo, S. Höfling, C.-Y. Lu, and J.-W. Pan, On-Demand Semiconductor Source of Entangled Photons Which Simultaneously Has High Fidelity, Efficiency, and Indistinguishability, Phys. Rev. Lett. **122,** 113602 (2019).

[47] J. Park, H. Kim, and H. S. Moon, Polarization-Entangled Photons from a Warm Atomic Ensemble Using a Sagnac Interferometer, Phys. Rev. Lett. **122,** 143601 (2019).

[48] J. Park, J. Bae, H. Kim, and H. S. Moon, Direct generation of polarization-entangled photons from warm atomic ensemble, Appl. Phys. Lett. **119,** 074001 (2021).

[49] J. Park and H. S. Moon, Generation of a bright four-photon entangled state from a warm atomic ensemble via inherent polarization entanglement, Appl. Phys. Lett. **120,** 024001 (2022).

[50] R. H. Brown and R. Q. Twiss, Correlation between photons in two coherent beams of light, Nature **177**, 27 (1956).

[51] F. Bouchard, A. Sit, Y. Zhang, R. Fickler, F. M. Miatto, Y. Yao, F. Sciarrino, and E. Karimi, Two-photon interference: the Hong–Ou–Mandel effect, Rep. Prog. Phys. **84**, 012402 (2021).

[52] H. Paul, Interference between independent photons, Rev. Mod. Phys. **58**, 209 (1986).

[53] S. Wengerowsky, S. K. Joshi, F. Steinlechner, H. Hübel, and R. Ursin, An entanglement-based wavelength-multiplexed quantum communication network, Nature **564**, 225 (2018).

[54] G.-T. Xue, Y.-F. Niu, X. Liu, J.-C. Duan, W. Chen, Y. Pan, K. Jia, X. Wang, H.-Y. Liu, Y. Zhang, P. Xu, G. Zhao, X. Cai, Y.-X. Gong, X. Hu, Z. Xie, and S. Zhu, Ultrabright Multiplexed Energy-Time-Entangled Photon Generation from Lithium Niobate on Insulator Chip, Phys. Rev. Appl. **15**, 064059 (2021).

[55] P. J. Mosley, J. S. Lundeen, B. J. Smith, and I. A. Walmsley, Conditional preparation of single photons using parametric downconversion: A recipe for purity, New J. Phys. **10**, 93011 (2008).

[56] C. C. Gerry and P. L. Knight, *Introductory Quantum Optics* (Cambridge University Press, Cambridge, 2005).

[57] Z.-Y. J. Ou, *Multi-Photon Quantum Interference* (Springer, New York, 2007), Vol. 43.

[58] P. J. Mosley, J. S. Lundeen, B. J. Smith, P. Wasylczyk, A. B. U'Ren, C. Silberhorn, and I. A. Walmsley, Heralded Generation of Ultrafast Single Photons in Pure Quantum States, Phys. Rev. Lett. **100**, 133601 (2008).